

# Hierarchical Collision Avoidance for Adaptive-Speed Multirotor Teleoperation

Kshitij Goel, Yves Georgy Daoud, Nathan Michael, and Wennie Tabib

**Abstract**—This paper improves safe motion primitives-based teleoperation of a multirotor by developing a hierarchical collision avoidance method that modulates maximum speed based on environment complexity and perceptual constraints. Safe speed modulation is challenging in environments that exhibit varying clutter. Existing methods fix maximum speed and map resolution, which prevents vehicles from accessing tight spaces and places the cognitive load for changing speed on the operator. We address these gaps by proposing a high-rate (10 Hz) teleoperation approach that modulates the maximum vehicle speed through hierarchical collision checking. The hierarchical collision checker simultaneously adapts the local map’s voxel size and maximum vehicle speed to ensure motion planning safety. The proposed methodology is evaluated in simulation and real-world experiments and compared to a non-adaptive motion primitives-based teleoperation approach. The results demonstrate the advantages of the proposed teleoperation approach both in time taken and the ability to complete the task without requiring the user to specify a maximum vehicle speed.

## I. INTRODUCTION

During cave search and rescue (CSAR), the Initial Response Team (IRT) executes a “hasty” search of the cave to provide rapid situational awareness (e.g., determining the probability of a victim’s location in various passages in the cave) [1]. This team may not have access to a prior map of the cave (e.g., there are 4378 documented caves in Virginia and only 1348 have been mapped) which makes searching for victims underground challenging [2]. Inaccessible areas (e.g., vertical ascents or tight passages) further complicate the situational awareness task. We envision teleoperated multirotor vehicles integrated into the IRT to rapidly search for victims, enhance the accessibility of the cave, and reduce the time taken to gain situational awareness. For example, a member of the IRT should be able to rapidly and safely teleoperate a multirotor through narrow passages. A key challenge for rapid CSAR is to reduce the cognitive load on the operator. To address this challenge, we develop a teleoperation methodology that adjusts the robot speed automatically based on environment complexity and perceptual constraints. Speed modulation in cave domains can be challenging due to varying clutter – open spaces can allow for high speeds but narrow passages require slow speeds to maintain safety. Allowing safety through narrow passages requires maintaining a local environment map and onboard collision checking assistance [3]. Depending on the resolution of the local environment map, narrow passages may or may not be visible to the collision checker. Thus, for

The authors are affiliated with the Robotics Institute, Carnegie Mellon University, USA

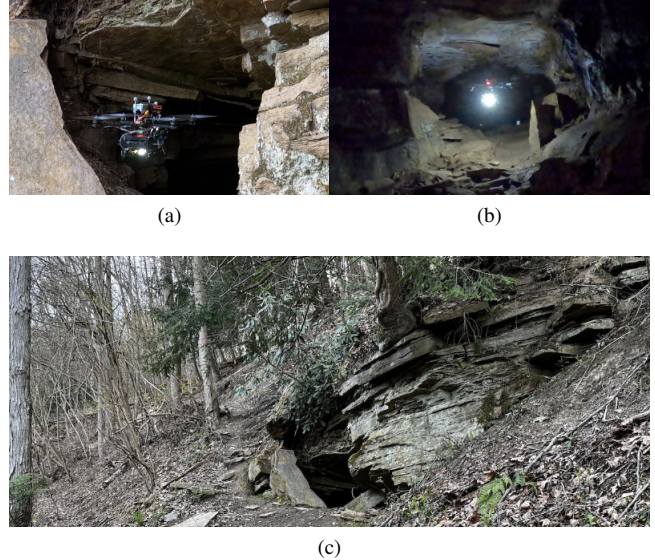


Fig. 1: Tele-operated multirotor adapts the motion planning speed and local map resolution to (a) enter a cave and (b) traverse a tight passage inside. (c) illustrates the surroundings near the cave entrance, which is embedded in a sloping hillside. A video of this experiment can be found at <https://youtu.be/VjyoPVXT8WY>.

teleoperation through narrow passages, variable-resolution local environment maps are required. Towards meeting the speed modulation and variable-resolution mapping requirements, the contributions of this paper are: (1) A hierarchical collision avoidance method that enables maximum speed modulation in a motion primitives-based teleoperation framework through updates to the map resolution and (2) evaluation of the method through simulated and real world experiments using a quadrotor, including one experiment in a wild cave (Fig. 1).

## II. RELATED WORK

Motion primitives-based teleoperation of a multirotor has been demonstrated to reduce operator cognitive load [4]. Spitzer et al. [3] propose a teleoperation approach that leverages a KD-Tree to locally represent the environment for fast collision checking. A motion primitive pruning approach leverages low-latency collision avoidance and the closest distance to the operator’s joystick input to allow for adaptive-speed teleoperation in the presence of obstacles. The local environment representation assumes the resolution of the map is fixed before the vehicle is teleoperated and does not encode unknown or free space information. However, in

practice, the unknown space information may be necessary to ensure safety when the environment is incrementally revealed through a limited range depth sensor [5, 6]. Free space information is necessary to simultaneously support applications such as robotic exploration [7]. Thus, in this work, we use probabilistic occupancy maps for local environment representation. A fixed resolution during operation imposes restrictions on the configuration space for the planner because the motion primitive pruning approach depends on the granularity of discretization. If the resolution is too low, the robot might not be able to enter narrow entrances due to the coarseness of the map. If the resolution is too high, the high perceptual latency of a fine map limits the maximum speed of the robot [8]. In this work, we address this research gap by proposing a multirotor teleoperation approach, which uses variable-resolution local probabilistic occupancy maps hierarchically to enable fast teleoperation in open spaces while ensuring safe, low-speed teleoperation through narrow passages.

Prior work in adaptive motion planning has been proposed to modulate robot speed based on application-specific heuristics. Zhang et al. [9] present a likelihood-based collision avoidance strategy for fast teleoperation of a multirotor by prioritizing open spaces for navigation to maintain high speed. The objective assumes that taking an alternate path (i.e., a path through open space) will lead to the same location as taking another (i.e., a path through a narrow passage); however, this assumption is flawed in the context of certain domains like caves. In contrast, our work adapts the maximum vehicle speed according to environment complexity. Quan et al. [10] propose an adaptive optimization-based motion planning approach for the multirotor navigation task, which is most similar to our approach. The heuristic used for speed modulation relies on the angle between the velocity direction and the gradient of the local signed distance field. This heuristic is coupled with a multi-layer model predictive control approach to allow for fast flight in sparsely cluttered environments and slow flight through dense clutter. However, while the motion planner allows adaptation in speed, the resolution of the environment representation is fixed. Selecting the resolution of an *a priori* unknown environment is difficult, which makes the approach of Quan et al. [10] unsuitable for our application. An alternative strategy is to operate with a range of voxel sizes for the local environment representation and modulate speeds according to the change in the map. The proposed approach builds on this strategy and introduces a motion primitive selection approach that modulates the maximum speed along the motion primitives according to the voxel size of the local occupancy map.

Several methods exist for hierarchical volumetric occupancy mapping. OctoMap by Hornung et al. [11] provides a multi-level representation of occupancy via an OcTree data structure. However, to the best of our knowledge, no motion planner exists that can leverage multiple levels of a local OctoMap-based representation to allow for adaptive-speed teleoperation through environments with varying clutter. Nelson et al. [12] present an occupancy grid adaptation method-

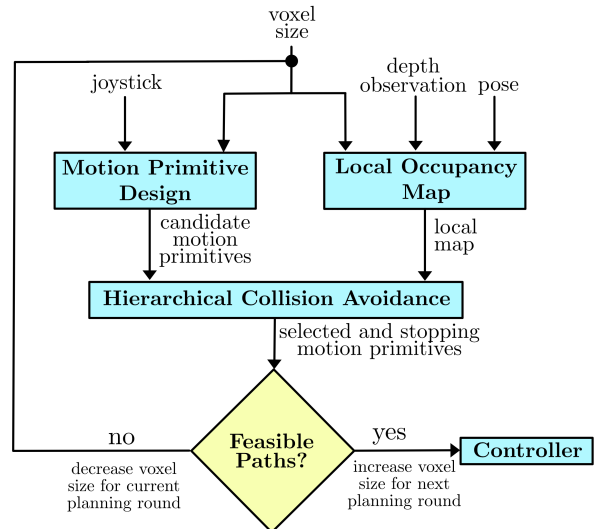


Fig. 2: Information flow diagram for the technical approach.

ology for two-dimensional environment exploration using ground robots. This approach is specific to the exploration scenario and the voxel sizes are adapted via the information-bottleneck method to minimize the cost of computing the exploration objective. It is unclear how this approach may be applied in the context of multirotor teleoperation since the objective highly depends on the intent of the human operator and may vary over time. Closest to our work, Funk et al. [13] create a multi-resolution OcTree-based representation for accurate 3D reconstruction and online planning. The resolution is selected by minimizing the error in occupancy representation. A path planning result is presented in this work that utilizes a “coarse-to-fine” approach for collision checking. The time to compute the motion plan varies from 0.01 s to 0.4 s depending on the desired start and end-points and the maximum resolution set by the user. However, the results are generated with post-processed datasets and a parallelized implementation so it is unclear how the performance would translate to compute constrained robotic systems and real-world results. A key consideration in the teleoperation context is to minimize the lag in the multirotor response felt by the operator by having a high motion planning rate. Thus, it is important to design a planning approach that maintains a steady planning rate in environments with varying clutter. The proposed approach addresses this gap by adapting a pre-specified number of map levels per planning round to achieve a planning rate of at least 10 Hz.

### III. TECHNICAL APPROACH

This section details the adaptive teleoperation approach. Figure 2 illustrates the components of the approach and how information flows between components. A local occupancy map is generated using depth observations, robot pose and voxel size (Sect. III-A). Note that due to the myopic nature of the teleoperation task, only a few recent observations are required to be included in the local occupancy map. The motion primitive design block takes input from the

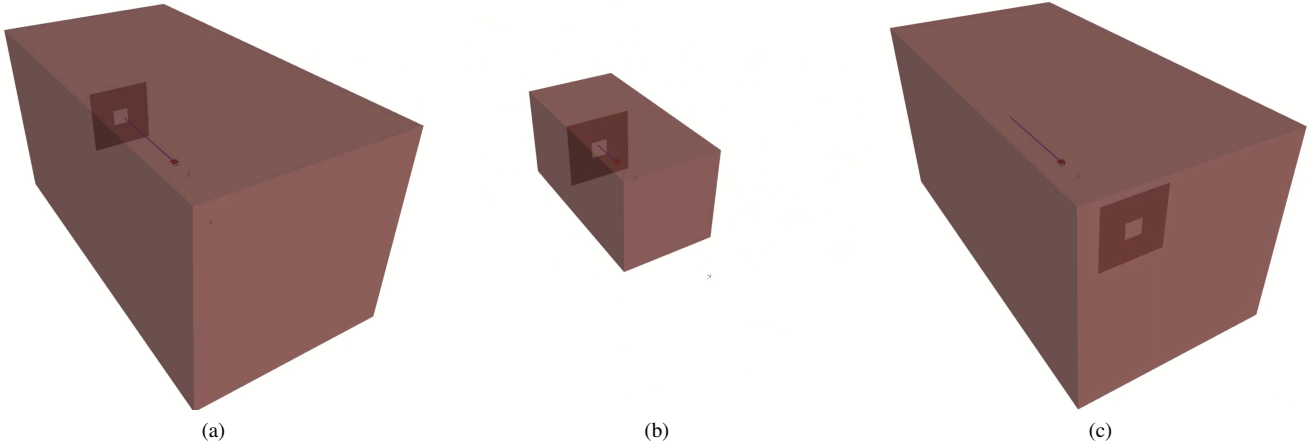


Fig. 3: Bounding box extents for a scenario where the robot traverses a window. The teleoperator gives maximum joystick input in the forward direction for these three figures. (a) When the robot is far from the window, the bounding box extents and local occupancy map are large because the voxel size is also large. (b) As the multirotor gets closer to the window, the voxel size decreases and so does the bounding box extent because the number of voxels in the map stays the same. (c) After exiting the window, the bounding box expands to the original size. Note that the change in bounding box extents is achieved by varying the voxel size and keeping the number of voxels constant.

operator’s joystick and the voxel size of the local occupancy map. This information is used to compute a candidate motion primitive close to the operator’s input and a fallback stopping motion primitive to use in case the next planning round fails (Sect. III-B). The hierarchical collision avoidance block takes as input these two motion primitives and the local map to perform collision checking (Sect. III-C). If both selected and stopping motion primitives are found to be feasible, they are sent to the controller for execution and the voxel size is increased for the next planning round. In case either of these primitives is infeasible, then the voxel size is decreased (and therefore the occupancy grid extents, see Fig. 3) and the process is repeated for the same planning round. If a suitable plan is not found, the stopping action from the previous planning round is executed.

#### A. Variable Resolution Local Occupancy Mapping

A three-dimensional local occupancy grid map  $\mathbf{m}$  is generated in the body frame  $\mathcal{B} = \{x_{\mathcal{B}}, y_{\mathcal{B}}, z_{\mathcal{B}}\}$  of the robot using the latest control state  $\mathbf{x}^c$  as the origin, voxel size  $\alpha$ , and number of voxels  $|\mathbf{m}| = N_x \times N_y \times N_z$ . The number of voxels along each dimension,  $\{N_x, N_y, N_z\}$ , are fixed throughout teleoperation but the voxel size  $\alpha$  may vary during or across planning rounds. The local occupancy grid bounding box  $\mathbf{B} = \{\mathbf{b}_{\min}, \mathbf{b}_{\max}\}$  extents are adjusted as a function of the voxel size,  $\alpha$ .  $\mathbf{b}_{\min} = \{x_{\min}, y_{\min}, z_{\min}\}$  is the minimum  $x_{\mathcal{B}} - y_{\mathcal{B}} - z_{\mathcal{B}}$  coordinate of the bounding box and  $\mathbf{b}_{\max} = \{x_{\max}, y_{\max}, z_{\max}\}$  is the maximum  $x_{\mathcal{B}} - y_{\mathcal{B}} - z_{\mathcal{B}}$  coordinate of  $\mathbf{B}$ . Each voxel  $m_i \in \mathbf{m}$  is a Bernoulli random variable whose value is 0 if it is free and 1 if it is occupied. Initially, the map is set to have a uniform occupancy probability in all voxels,  $p(m_i) = 0.5, \forall i \in \{1, \dots, |\mathbf{m}|\}$ .

It is assumed that the multirotor is equipped with a limited field-of-view (FoV) forward-facing depth camera

that provides a dense depth measurement  $\mathcal{Z}$  at a user-specified sensing rate  $1/\Delta t_s$ . In addition to the latest state-measurement pair (“keyframe”),  $\mathcal{K}_l = \{\mathbf{x}_l^c, \mathcal{Z}_l\}$ , one past keyframe is maintained  $\mathcal{K}_p = \{\mathbf{x}_p^c, \mathcal{Z}_p\}$ . The past keyframe is selected based on a Euclidean distance threshold  $\beta$  between the latest state  $\mathbf{x}_l^c$  and the previous keyframe state  $\mathbf{x}_p^c$ . Measurement  $\mathcal{Z}_p$  is transformed into the frame of reference of the keyframe  $\mathcal{K}_l$ . The occupancy map is updated using both  $\mathcal{Z}_l$  and the transformed  $\mathcal{Z}_p$  through the standard logodds update [14]. If the voxel size  $\alpha$  changes during the planning round, the occupancy grid map is regenerated using  $\mathcal{Z}_l$  and  $\mathcal{Z}_p$  using the new  $\alpha$ . The time complexity of this regeneration step depends on the total number of voxels. In practice, we decide the number of voxels based on the available compute and keep them fixed throughout teleoperation.

The local occupancy map  $\mathbf{m}$  partitions the space  $\mathbb{R}^3$  into three subspaces: (1) free space  $\mathcal{X}_{\text{free}}$ , (2) occupied space  $\mathcal{X}_{\text{occ}}$ , and (3) unknown space  $\mathcal{X}_{\text{unk}}$ . To ensure safety, the motion plans sent to the robot must lie in free space,  $\mathbf{x}_t \in \mathcal{X}_{\text{free}}$ , for all time  $t$ . To check the motion plans against  $\mathcal{X}_{\text{unsafe}} = \{\mathcal{X}_{\text{occ}} \cup \mathcal{X}_{\text{unk}}\}$ , a common strategy is to compute a discrete distance field  $\mathbf{d}$  where each point in the field stores the shortest distance to  $\mathcal{X}_{\text{unsafe}}$ . We use the variant of the fast-marching method by Sethian [15] over occupancy grids to compute the distance map  $\mathbf{d}$  from the local map  $\mathbf{m}$ . It is assumed that the robot can fit a cube of side-length  $2 \cdot r_{\text{robot}}$  and a  $r_{\text{coll}}$  amount of tolerance from  $\mathcal{X}_{\text{unsafe}}$  is required for safety.

#### B. Motion Primitive Design

We use the control input parameterization by Yang et al. [4] that maps the space of joystick inputs to a finite set of forward-arc motion primitives. The joystick input is represented as  $\mathbf{a}_t = \{v_{x,t}, v_{z,t}, \omega_t\}$ , where  $v_{x,t}$  is the velocity command in the  $x_{\mathcal{B}}$  direction,  $v_{z,t}$  is the velocity command

in the  $z_B$  direction, and  $\omega_t$  is the angular velocity command around the  $z_B$  direction. All velocity commands are uniformly dense sets clamped with user-specified bounds:  $v_{x,t} \in [-V_x, V_x]$ ,  $v_{z,t} \in [-V_z, V_z]$ , and  $\omega_t \in [-\Omega, \Omega]$ . Assuming a user-specified duration of the motion primitive,  $T$ , a forward-arc motion primitive  $\gamma_t = \{\mathbf{a}_t, T\}$  can be generated by propagating the unicycle model [16]. The motion primitive  $\gamma_t$  is checked for feasibility and sent to the controller for execution.

Prior motion primitives-based teleoperation frameworks that utilize forward-arc motion primitives assume velocity command bounds to be constant and user-specified [3, 4]. These bounds can influence the design of the motion primitives when they are used for navigation in unknown environments. Such design decisions are made to ensure that the robot never enters an inevitable collision state [5]. For example, setting the  $x_B$ -velocity bound,  $V_x$ , depends on many factors: (1) mapping time ( $\Delta t_m$ ), (2) planning time ( $\Delta t_p$ ), (3) sensing time ( $\Delta t_s$ ), (3) sensing range ( $z_{\max}$ ), (4) collision tolerance distance ( $r_{\text{coll}}$ ), (5) robot radius ( $r_{\text{robot}}$ ), and (6) maximum  $x_B$ -deceleration ( $A_x$ ) [17]. For the teleoperation task, we also need to account for the bounding box  $\mathbf{B}$  of the local occupancy map  $\mathbf{m}$ . In terms of the voxel size and the number of voxels, the corners of the local map bounding box  $\mathbf{B}$  are given by  $\mathbf{b}_{\min} = -(\alpha/2) \cdot \{N_x, N_y, N_z\}$  and  $\mathbf{b}_{\max} = (\alpha/2) \cdot \{N_x, N_y, N_z\}$ . Since the robot is at the center of  $\mathbf{B}$ , the map information available in front of the robot is up to a distance  $z_{\text{eq}} = \min(z_{\max}, (\alpha/2)N_x)$  from the robot. Thus, an ideal upper bound for the maximum  $x_B$ -velocity is derived using Euler motion equations as:

$$V_x = A_x \left( \sqrt{\Delta t_l^2 + 2 \frac{z_{\text{eq}} - (r_{\text{robot}} + r_{\text{coll}})}{A_x}} - \Delta t_l \right), \quad (1)$$

where,  $\Delta t_l = \Delta t_s + \Delta t_m + 2\Delta t_p$ . This equation represents an ideal upper bound because it assumes the deceleration  $A_x$  is attained instantly and does not consider the motor dynamics. Therefore, in practice, we reduce  $V_x$  with a constant  $\delta v$  to account for these unmodeled factors.

Note that Eq. (1) represents the velocity bound in terms of the voxel size  $\alpha$  of the local occupancy map  $\mathbf{m}$ . Thus, the velocity bound should scale according to the resolution of the map. Consequently, the motion primitive design is dependent on the voxel size. We use this fact to adapt voxel size and the motion primitive design across and within planning rounds through hierarchical collision avoidance (Sect. III-C).

### C. Hierarchical Collision Avoidance

Algorithm 1 shows the pseudocode for the Hierarchical Collision Avoidance (HCA) algorithm. Instead of using a fixed voxel size  $\alpha$  for the local occupancy map  $\mathbf{m}$  throughout teleoperation, it is adapted hierarchically based on the output of the collision checker. At the start of the planning round, the voxel size  $\alpha$  is set  $\Delta\alpha$  above the one used in the previous planning round,  $\alpha_{\text{prev}}$ , but clamped by a pre-specified  $\alpha_{\max}$  and  $\alpha_{\min}$  (Line 2). The motion primitive design is updated for this voxel size (Sect. III-B, Line 5). The joystick input

---

### Algorithm 1: Hierarchical Collision Avoidance

---

```

1 function HCA ( $\mathbf{x}_{t+\Delta t_p}$ ,  $\mathbf{a}$ ,  $\alpha_{\text{prev}}$ )
   input:  $\mathbf{x}_{t+\Delta t_p}$ ,  $\mathbf{a}$ ,  $\alpha_{\text{prev}}$ 
   parameters:  $\alpha_{\max}$ ,  $\alpha_{\min}$ ,  $\Delta\alpha$ ,  $\Delta t_p$ ,  $\Delta t_m$ ,  $\Delta t_s$ ,
                  $N_x$ ,  $N_y$ ,  $N_z$ 
   output:  $\gamma_{\text{sel}}$ ,  $\gamma_{\text{stop}}$ ,  $\alpha_{\text{prev}}$ 
2    $\alpha \leftarrow \min(\max(\alpha_{\text{prev}} + \Delta\alpha, \alpha_{\min}), \alpha_{\max})$ 
3    $\Delta l \leftarrow 0$ 
4   while  $\Delta l \leq 2$  do
5      $V_x \leftarrow \text{MaxSpeed}(\mathbf{m}, \Delta t_p, \Delta t_m, \Delta t_s)$ 
6      $\gamma_{\text{sel}} \leftarrow \text{MapJoystick}(\mathbf{x}_{t+\Delta t_p}, \mathbf{a}, V_x)$ 
7      $\gamma_{\text{stop}} \leftarrow \text{StoppingAction}(\gamma_{\text{sel}}, \Delta t_p)$ 
8      $\mathbf{m} \leftarrow \text{LocalMap}(\alpha, N_x, N_y, N_z)$ 
9      $\mathbf{d} \leftarrow \text{DistanceField}(\mathbf{m})$ 
10    if  $\text{InCollision}(\gamma_{\text{sel}}, \gamma_{\text{stop}}, \mathbf{d})$  then
11       $\alpha \leftarrow \min(\max(\alpha - \Delta\alpha, \alpha_{\min}), \alpha_{\max})$ 
12       $\Delta l \leftarrow \Delta l + 1$ 
13    else
14      break
15    end
16  end
17   $\alpha_{\text{prev}} \leftarrow \alpha$ 
18  if  $\Delta l > 2$  then
19    return  $\alpha_{\text{prev}}$ 
20  else
21    return  $\gamma_{\text{sel}}$ ,  $\gamma_{\text{stop}}$ ,  $\alpha_{\text{prev}}$ 
22  end
23 end

```

---

is mapped to the closest motion primitive,  $\gamma_{\text{sel}}$ , via grid search [4] (Line 6). A stopping motion primitive,  $\gamma_{\text{stop}}$ , is generated as a fallback action in case the next planning round fails (Line 7). The distance field (Sect. III-A, Line 9) generated via the local map at the voxel size  $\alpha$  (Sect. III-A, Line 8) is used for collision checking. If either  $\gamma_{\text{sel}}$  or  $\gamma_{\text{stop}}$  are in collision (Line 10), we reduce the voxel size by  $\Delta\alpha$  (Line 11), and try planning again. The map generation step contributes the most to the time complexity of this algorithm. If a feasible plan is found within a maximum of three map level changes (Line 18), it is returned (Line 21) and the next plan is executed. We choose to limit the checks to three map levels at a time to keep a consistent time complexity across planning rounds. If a feasible plan is still not possible, the current voxel size is returned as  $\alpha_{\text{prev}}$  (Line 19) to use in the next planning round, and the previously planned stopping action is executed.

### D. Implementation Detail

The proposed framework is deployed to the aerial system of dimensions  $0.6\text{ m} \times 0.3\text{ m} \times 0.3\text{ m}$  and mass  $2.5\text{ kg}$  (Fig. 4). This design is an improved version of the robot from [7] with a higher motor constant, longer flight time, and larger depth sensing range (Intel Realsense D455). The onboard companion computers, state estimation system, the control system remain the same.



Fig. 4: The robot used in the field experiments is equipped with a forward-facing Intel Realsense D455, downward-facing mvBluefox global shutter color camera, and Pixracer flight controller.

Parameter	Value	Parameter	Value
$\Delta t_p$	0.1 s	$N_y$	20
$\Delta t_m$	0.08 s	$N_z$	20
$\Delta t_s$	0.07 s	$z_{\max}$	10.0 m
$\Delta \alpha$	0.01 m	$r_{\text{robot}}$	0.3 m
$N_x$	40	$r_{\text{coll}}$	0.1 m

TABLE I: Parameters common to all experiments.

The parameters common to all the experiments are listed in Tab. I. These parameters remain constant throughout teleoperation. Note that the operator does not need to specify a maximum velocity parameter found in most multirotor motion planning frameworks. Instead, the maximum velocity is determined in each planning round based on the local map extents (Sect. III-B). Note that the  $\Delta \alpha$  parameter specifies the change in map resolution after each collision checking iteration. Thus, this parameter should be specified based on the desired planning rate and the available onboard compute.

#### IV. RESULTS

The adaptive teleoperation framework with hierarchical collision avoidance is implemented with a single thread on a CPU in C++ with the Robot Operating System (ROS) middleware. A 3.7 GHz Intel Core i9-10900K CPU with 32 GB RAM is used for the simulation experiments. A 1.8 GHz Intel Core i7-8550U CPU with 32 GB RAM is used for the hardware experiments. We evaluate the approach with four teleoperation scenarios, two for simulation experiments (*Window Scenario*, *Varying-Clutter Cave Scenario*) and two for hardware experiments (*Door Scenario*, *Cave Scenario*). Experimentation for the Cave Scenario occurred at a cave on the Barbara Schomer Cave Preserve in Clarion County, PA.

##### A. Simulation Experiments

*Window Scenario:* A multirotor is placed 10 m away from a simulated window of dimensions  $0.9 \text{ m} \times 0.9 \text{ m}$  (Fig. 5a). The operator intends to fly the multirotor in the forward direction, through the window, at the maximum possible speed (Fig. 5b). The teleoperation task is successful if the multirotor passes through the window without collisions and without the operator having to lower the raw joystick input. Three teleoperation methodologies are compared: (1) the proposed adaptive approach with  $\alpha_{\max} = 0.5 \text{ m}$  and

$\alpha_{\min} = 0.1 \text{ m}$ ; (2) a non-adaptive approach with a fixed voxel size,  $\alpha_1 = 0.2 \text{ m}$ ; and (3) a non-adaptive approach with a fixed voxel size,  $\alpha_2 = 0.5 \text{ m}$ . These parameters are chosen such that for  $\alpha_1 = 0.2 \text{ m}$  the local map is fine enough for the window to be visible while  $\alpha_2 = 0.5 \text{ m}$  leads to a local map that is too coarse for it.

The results for the *Window Scenario* are shown in Fig. 5. We plot the speed and the local map voxel size over the  $X$  coordinate with respect to the window ( $X = 0$ ) in Figs. 5c and 5d respectively. For the non-adaptive case with  $\alpha_1 = 0.2 \text{ m}$  voxel size, the operator teleoperates the multirotor through the window without collision at a constant speed of  $1.17 \text{ m/s}$ . For the non-adaptive case with  $\alpha_2 = 0.5 \text{ m}$ , the operator is not able to teleoperate the multirotor through the window while achieving a top speed of  $3.03 \text{ m/s}$  in open space. For the adaptive case, the operator can teleoperate through the window while being able to achieve a top speed of  $3.03 \text{ m/s}$  in open space, automatically slowing down to move through the window, and attaining the same top speed after passing through the window. The automatic slow down is expected due to the adaptation in the local map voxel size from  $\alpha_{\max} = 0.5 \text{ m}$  down to  $0.25 \text{ m}$ . Thus, the proposed approach allows speed modulation without requiring the operator to adjust the joystick input. Note that the speed attained close to the window in the adaptive case is lower than the constant speed of  $1.17 \text{ m/s}$  achieved in the non-adaptive  $0.2 \text{ m}$  voxel size case. This is because the length of the motion primitive when the robot is decelerating is longer than the case when the robot is moving at a constant speed. The collision checker marks the longer motion primitive infeasible, which results in a speed modulation that decelerates the robot to lower than  $1.17 \text{ m/s}$ . This behavior may be changed through a collision checker that utilizes the higher derivatives of position, but this is left as future work.

*Varying-Clutter Cave Scenario:* A multirotor is placed in a simulated cave environment containing varying amounts of clutter (Fig. 6a). Region 1 is an open space, so the expected operation is high-speed multirotor teleoperation. Region 2 is a cluttered space where speeds must be reduced to ensure safety. Region 3 contains a narrow entrance to a larger passage that must be visible in the local occupancy map to enable robot access. The teleoperation task is to fly from Region 1 to Regions 2 and 3 and return to Region 1 (Fig. 6b). The operator supplies the directional inputs from the joystick but the forward speed input is always the maximum value. The three teleoperation methods from the *Window Scenario* are used here without modification in parameters. The methods are compared based on: (1) whether they allow access to all three regions and (2) the total time taken for the teleoperation task. Figures 6c to 6e show the variation of the speed over time for each of the methods. Without adaptation, the method with a high voxel size can traverse Region 1 at high speeds and can enter Region 2 partially. However, it is unable to access the other regions. When the voxel size is lower or adaptive, the operator can teleoperate through all regions and return to Region 1. However, without adaptation, the speeds are lower compared

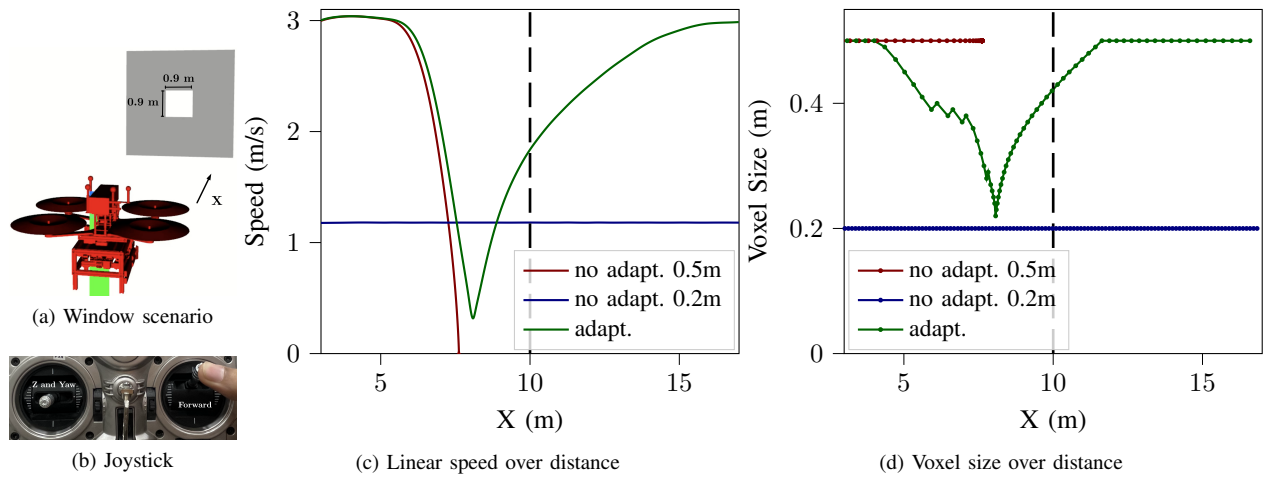
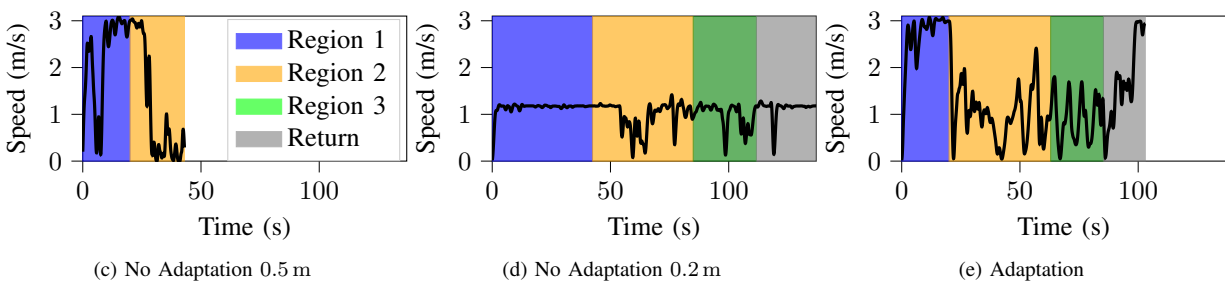
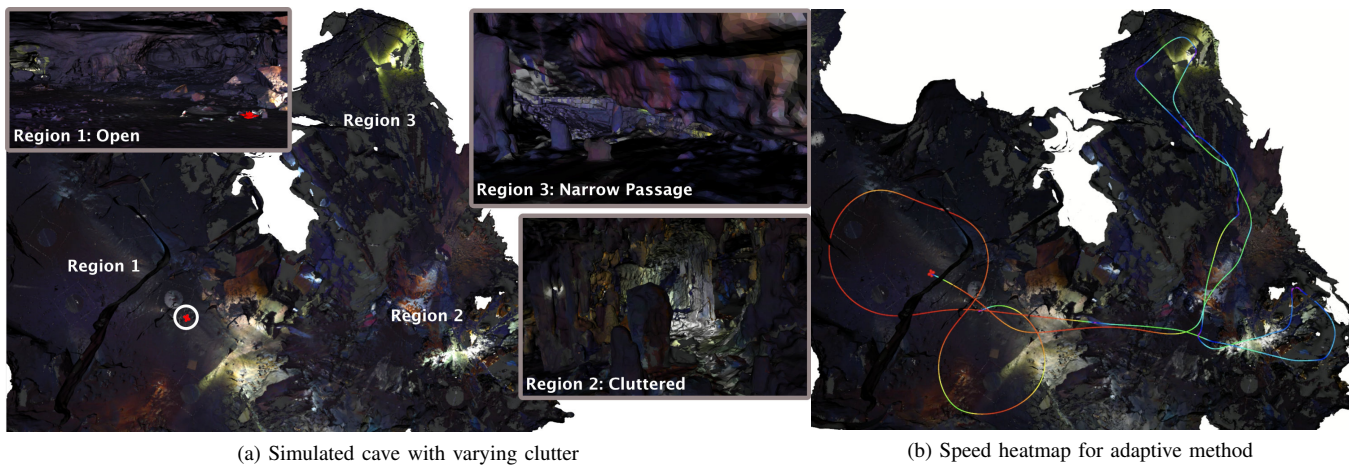


Fig. 5: Performance comparison for the simulated window teleoperation task. (a) depicts the initial conditions for the task. A multirotor hovers at a distance of 10 m from a window of dimensions 0.9 m  $\times$  0.9 m. The operator controls the multirotor via the joystick shown in (b). The operator intends to go forward at the highest speed possible. (c) and (d) show the variation of the forward speed and the local map voxel size as a function of the distance from the window for the three teleoperation approaches.



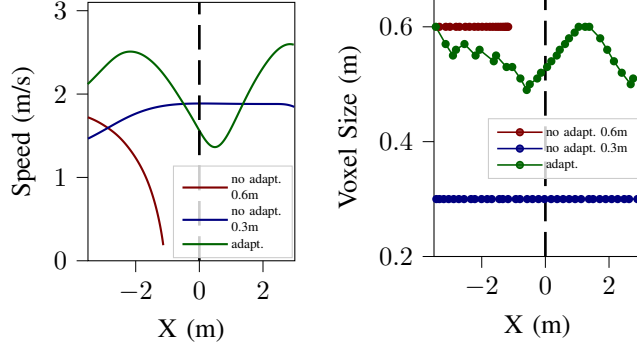
Method	Region 1		Region 2		Region 3		Return	
	Time (s)	Avg. Speed (m/s)	Time (s)	Avg. Speed (m/s)	Time (s)	Avg. Speed (m/s)	Time (s)	Avg. Speed (m/s)
No adapt. 0.5 m	<b>20.0</b>	2.22	–	–	–	–	–	–
No adapt. 0.2 m	42.4	1.15	43.2	0.98	26.7	<b>0.97</b>	25.3	1.13
<b>Adaptation</b>	<b>20.0</b>	<b>2.67</b>	<b>43.0</b>	<b>1.02</b>	<b>22.3</b>	0.93	<b>17.7</b>	<b>1.69</b>

(f) Comparison of teleoperation statistics

Fig. 6: Performance comparison for the (a) varying-clutter cave scenario with three different spaces: Region 1 is an open space, Region 2 is cluttered, and Region 3 is a narrow passage. The speeds achieved by the robot for each method are plotted over time in (c), (d), and (e). The graphs and the table in (f) demonstrate that the (c) No Adaptation 0.5 m variant cannot complete the circuit, while both the (d) No Adaptation 0.2 m and (e) Adaptation variants successfully traverse all regions. Our method completes the circuit in the least time while modulating speeds, as illustrated in the heatmap in (b). A video of this experiment can be found at <https://youtu.be/VjyoPVXT8WY>.



(a) Door scenario



(b) Linear speed over distance

(c) Voxel size over distance

Fig. 7: Performance comparison for the door teleoperation task. (a) a robot starts at hover from outside a building and the operator intends to enter the building at the maximum possible forward speed (Fig. 5b) through a door of width 0.9 m. (b) and (c) show the speeds and voxel sizes as a function of distance from the door. A video of this experiment can be found at <https://youtu.be/VjyoPVXT8WY>.

to the adaptive-speed case. Consequently, the total time taken for the non-adaptive 0.2 m case is 137 s versus 103 s for the adaptive-speed case. Figure 6f shows the distribution of the time taken with the different phases of the teleoperation task. The adaptive-speed method achieves lower times and higher average speeds in most phases. These results demonstrate the efficacy of the proposed method in environments with varying amounts of clutter.

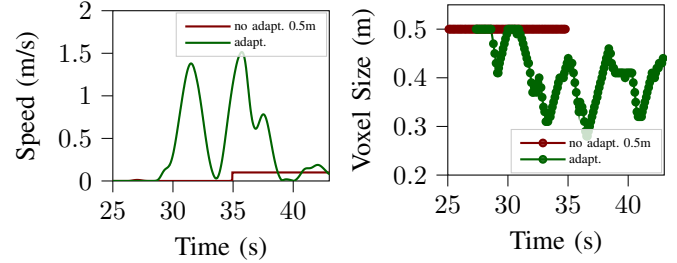
### B. Real-World Experiments

*Door Scenario:* A multirotor is hovering outside a building, about 12 m away from a door, which has a frame with a 0.9 m width (Fig. 7a). The operator’s intent and the measures of success are the same as in the *Window Scenario*, this time flying through the door to enter the building. The same teleoperation methodologies are compared as in the *Window Scenario*, with  $\alpha_{\max} = 0.6$  m,  $\alpha_{\min} = 0.3$  m,  $\alpha_1 = 0.3$  m, and  $\alpha_2 = 0.6$  m. The choice of these parameters is motivated by the same reasons as in the *Window Scenario*.

The results for the *Door Scenario* are shown in Fig. 7. Just like the *Window Scenario*, the speed and local map voxel sizes are plotted against the distance from the door ( $X = 0$ ) in Figs. 7b and 7c, respectively. We observe similar results as in the *Window Scenario*. For the non-adaptive case with  $\alpha_1 = 0.3$  m, the operator can teleoperate through the door at a constant speed of 1.88 m/s. For the non-adaptive case with  $\alpha_1 = 0.6$  m, the operator is not able to teleoperate through the door while achieving high speeds outside the building. For the adaptive case, the



(a) Cave scenario



(b) Linear speed over time

(c) Voxel size over time

Fig. 8: Performance comparison for the cave teleoperation task. (a) a robot starts at hover from a relatively spacious part of a cave passage. The operator intends to go through the passage at the maximum possible forward speed (Fig. 5b). (b) and (c) show the speeds and map voxel sizes as a function of time. Without map adaptation, the robot is unable to go through the narrow passage and the operator must land the robot around the 35 s mark. With map adaptation, the speeds are adapted according to the environment complexity and the robot traverses the narrow passage. A video of this experiment can be found at <https://youtu.be/VjyoPVXT8WY>.

operator can teleoperate through the door while being able to achieve a maximum speed of 2.50 m/s outside the building, automatically slowing down at the door and achieving the same maximum speed again after entering the building. Thus, the *Door Scenario* experiment demonstrates the efficacy of the proposed teleoperation method on the computationally-constrained multirotor system shown in Fig. 4.

*Cave Scenario:* A multirotor hovers in a narrow passage inside of the wild cave shown in Fig. 1c. The operator intends to fly through the narrow passage without substantially altering the raw joystick input. Two teleoperation methodologies are compared in this case: (1) the adaptive approach with  $\alpha_{\max} = 0.5$  m,  $\alpha_{\min} = 0.1$  m and (2) the non-adaptive approach with  $\alpha = 0.5$  m.

The results for the *Cave Scenario* are shown in Fig. 8. In the no-adaptation case with  $\alpha = 0.5$  m, the operator is not able to teleoperate the multirotor through the narrow passage of the cave due to the coarse local map. However, for the adaptation case, the voxel size is reduced automatically to allow for a finer local map for flight through the narrow passage. Thus, the proposed approach allows teleoperation through a narrow passage where it is difficult to guess the required voxel size of the local map before starting teleoperation.

Table II illustrates the mean and standard deviation for total planning times for the real-world experiments. As noted in Sect. III-C, most of the time complexity of the proposed approach is due to local map generation. Imposing an upper

Method	Door Scenario	Cave Scenario
No adapt. low vox. size	0.06 s $\pm$ 0.01 s	–
No adapt. high vox. size	0.03 s $\pm$ 0.01 s	0.04 s $\pm$ 0.01 s
Adaptation	0.06 s $\pm$ 0.03 s	0.06 s $\pm$ 0.03 s

TABLE II: Planning times for the real-world experiments.

bound on the number of local map generation steps per planning round enables us to contain that time complexity and achieve a consistent planning rate (i.e., the low standard deviation in planning time).

## V. LIMITATIONS

The framework assumes that the operator is aiming for the center line a narrow passage when teleoperating through it. While the forward speed input is not required, additional gains in performance can be achieved through a pruning approach to assist with directional inputs [3]. Further, the maximum speed bound calculation applies to holonomic teleoperation only if a depth sensor is pointed in the sideways direction. When multiple depth cameras are available on the platform, the maximum velocity in the sideways direction can be calculated according to Eq. (1) but for the  $y_B$  and  $-y_B$  directions.

## VI. CONCLUSION

A human operator teleoperating an aerial system in a CSAR scenario may experience a high cognitive load while modulating the robot’s speed to safely navigate through varying environment clutter. This paper detailed an approach for automatic maximum speed modulation for teleoperation of a multirotor in environments consisting of open, cluttered, and narrow spaces. We couple the motion primitive design and variable-resolution mapping to create a hierarchical collision avoidance method that modulates the maximum speed and voxel size of the local occupancy map simultaneously depending on the environment complexity. The framework is experimentally evaluated both in simulation and real-world complex environments, including caves, demonstrating that the speed and map resolution adaptation yields advantages both in terms of time taken and ability to complete a task. For future work, we plan to extend this work to combine with directional input assistance.

## VII. ACKNOWLEDGMENTS

The authors thank the Mid Atlantic Karst Conservancy for granting permission to test at a cave on the Barbara Schomer Cave Preserve. The authors also thank D. Wettergreen and S. Vats for their feedback on this manuscript.

## REFERENCES

- [1] John C. Hempel and Annette Fregeau-Conover. *On Call: A Complete Reference for Cave Rescue*. National Speleological Society, 2001. ISBN 978-1-879961-16-6.
- [2] Alejandro C Stella-Watts, Christopher P Holstege, Jae K Lee, and Nathan P Charlton. The epidemiology of caving injuries in the United States. *Wilderness & environmental medicine*, 23(3):215–222, 2012.
- [3] Alex Spitzer, Xuning Yang, John Yao, Aditya Dhawale, Kshitij Goel, Mosam Dabhi, Matt Collins, Curtis Boirum, and Nathan Michael.

- Fast and Agile Vision-Based Flight with Teleoperation and Collision Avoidance on a Multirotor. In Jing Xiao, Torsten Kröger, and Oussama Khatib, editors, *Proceedings of the 2018 International Symposium on Experimental Robotics*, Springer Proceedings in Advanced Robotics, pages 524–535, Cham, 2020. Springer International Publishing. ISBN 978-3-030-33950-0. doi: 10.1007/978-3-030-33950-0.45.
- [4] Xuning Yang, Koushil Sreenath, and Nathan Michael. A framework for efficient teleoperation via online adaptation. In *2017 IEEE International Conference on Robotics and Automation (ICRA)*, pages 5948–5953, May 2017. doi: 10.1109/ICRA.2017.7989701.
- [5] Lucas Janson, Tommy Hu, and Marco Pavone. Safe Motion Planning in Unknown Environments: Optimality Benchmarks and Tractable Policies. In *Robotics: Science and Systems XIV*. Robotics: Science and Systems Foundation, June 2018. ISBN 978-0-9923747-4-7. doi: 10.15607/RSS.2018.XIV.061. URL <http://www.roboticsproceedings.org/rss14/p61.pdf>.
- [6] Jesus Tordesillas, Brett T. Lopez, Michael Everett, and Jonathan P. How. FASTER: Fast and Safe Trajectory Planner for Navigation in Unknown Environments. *IEEE Transactions on Robotics*, pages 1–17, 2021. ISSN 1941-0468. doi: 10.1109/TRO.2021.3100142.
- [7] Wennie Tabib, Kshitij Goel, John Yao, Curtis Boirum, and Nathan Michael. Autonomous Cave Surveying With an Aerial Robot. *IEEE Transactions on Robotics*, pages 1–17, 2021. ISSN 1552-3098, 1941-0468. doi: 10.1109/TRO.2021.3104459. URL <https://ieeexplore.ieee.org/document/9536757/>.
- [8] Davide Falanga, Suseong Kim, and Davide Scaramuzza. How Fast Is Too Fast? The Role of Perception Latency in High-Speed Sense and Avoid. *IEEE Robotics and Automation Letters*, 4(2):1884–1891, April 2019. ISSN 2377-3766. doi: 10.1109/LRA.2019.2898117.
- [9] Ji Zhang, Chen Hu, Rusht Gupta Chadha, and Sanjiv Singh. Falco: Fast likelihood-based collision avoidance with extension to human-guided navigation. *Journal of Field Robotics*, 37(8):1300–1313, 2020. ISSN 1556-4967. doi: 10.1002/rob.21952. URL <https://onlinelibrary.wiley.com/doi/abs/10.1002/rob.21952>.
- [10] Lun Quan, Zhiwei Zhang, Xingguang Zhong, Chao Xu, and Fei Gao. EVA-Planner: Environmental Adaptive Quadrotor Planning. In *2021 IEEE International Conference on Robotics and Automation (ICRA)*, pages 398–404, May 2021. doi: 10.1109/ICRA48506.2021.9561759.
- [11] Armin Hornung, Kai M. Wurm, Maren Bennewitz, Cyrill Stachniss, and Wolfram Burgard. OctoMap: An efficient probabilistic 3D mapping framework based on octrees. *Autonomous Robots*, 34(3):189–206, April 2013. ISSN 1573-7527. doi: 10.1007/s10514-012-9321-0. URL <https://doi.org/10.1007/s10514-012-9321-0>.
- [12] Erik Nelson, Micah Corah, and Nathan Michael. Environment model adaptation for mobile robot exploration. *Autonomous Robots*, 42(2):257–272, February 2018. ISSN 0929-5593, 1573-7527. doi: 10.1007/s10514-017-9669-2. URL <http://link.springer.com/10.1007/s10514-017-9669-2>.
- [13] Nils Funk, Juan Tarrio, Sotiris Papatheodorou, Marija Popović, Pablo F. Alcantarilla, and Stefan Leutenegger. Multi-Resolution 3D Mapping With Explicit Free Space Representation for Fast and Accurate Mobile Robot Motion Planning. *IEEE Robotics and Automation Letters*, 6(2):3553–3560, April 2021. ISSN 2377-3766. doi: 10.1109/LRA.2021.3061989.
- [14] Sebastian Thrun. Probabilistic robotics. *Communications of the ACM*, 45(3):52–57, March 2002. ISSN 0001-0782, 1557-7317. doi: 10.1145/504729.504754. URL <https://dl.acm.org/doi/10.1145/504729.504754>.
- [15] J A Sethian. A fast marching level set method for monotonically advancing fronts. *Proceedings of the National Academy of Sciences of the United States of America*, 93(4):1591–1595, February 1996. ISSN 0027-8424. URL <https://www.ncbi.nlm.nih.gov/pmc/articles/PMC39986/>.
- [16] Mihail Pivtoraiko, Issa A.D. Nesnas, and Alonzo Kelly. Autonomous robot navigation using advanced motion primitives. In *2009 IEEE Aerospace Conference*, pages 1–7, March 2009. doi: 10.1109/AERO.2009.4839309.
- [17] Kshitij Goel, Micah Corah, Curtis Boirum, and Nathan Michael. Fast Exploration Using Multirotors: Analysis, Planning, and Experimentation. In Genya Ishigami and Kazuya Yoshida, editors, *Field and Service Robotics*, Springer Proceedings in Advanced Robotics, pages 291–305, Singapore, 2021. Springer. ISBN 9789811594601. doi: 10.1007/978-981-15-9460-1.21.